water

MDPI

Article

Geochemical and Mineralogical Characterisation of Carbonate-Rich Lake Sediments from Lake Kolon, Hungary

Tamás Zsolt Vári *, Gábor Bozsó, Pál Sümegi and Elemér Pál-Molnár

Department of Geology, University of Szeged, 2-6 Egyetem Street, H-6722 Szeged, Hungary; bozso.gabor@geo.u-szeged.hu (G.B.); sumegi@geo.u-szeged.hu (P.S.); palm@geo.u-szeged.hu (E.P.-M.)
* Correspondence: varitamaszsolt@gmail.com

Abstract

The Danube–Tisza Interfluve in central Hungary, a key region for Quaternary paleoenvironmental reconstruction, hosts ephemeral saline lakes that serve as highly sensitive archives of past climate variability but are increasingly threatened by desertification. Carbonate-rich lacustrine deposits within these systems form through a complex interplay of biogenic CO_2 uptake and inorganic precipitation driven by evaporation. To refine paleoenvironmental reconstructions from these archives, a lacustrine sediment core was analysed using XRPD for mineralogy and XRF for major and trace element geochemistry. The results reveal four distinct environmental phases: a cold, siliciclastic-dominated Late Glacial period (c. 23,600–13,400 cal BP); an abrupt shift to massive autogenic carbonate production during the warmer Late Glacial Interstadial, which was also marked by intense aeolian activity (Zr enrichment); the development of a Holocene fen (from c. 11,200 cal BP) with fluctuating hydrology; and a recent interval (from c. 800 cal BP) showing extreme enrichment in phosphorus, lead, and sulphur from anthropogenic sources.

Keywords: quaternary period; saline lake; lacustrine sediment; freshwater carbonate; geochemistry; mineralogy

check for updates

Academic Editor: Barbara Futa

Received: 28 August 2025
Revised: 23 September 2025
Accepted: 26 September 2025
Published: 26 September 2025

Citation: Vári, T.Z.; Bozsó, G.; Sümegi, P.; Pál-Molnár, E. Geochemical and Mineralogical Characterisation of Carbonate-Rich Lake Sediments from Lake Kolon, Hungary. *Water* **2025**, *17*, 2830. https://doi.org/10.3390/w17192830

Copyright: © 2025 by the authors. Licensee MDPI, Basel, Switzerland. This article is an open access article distributed under the terms and conditions of the Creative Commons Attribution (CC BY) license (https://creativecommons.org/licenses/by/4.0/).

1. Introduction

Evidence of the Quaternary period's changing climate and environment is preserved in continental deposits and landscape forms. Within the Carpathian Basin, the Danube–Tisza Interfluve in Hungary stands out as a key area for the paleoenvironmental reconstruction. This region, among numerous sand formations and loess sequences, hosts shallow, ephemeral wetlands and saline lakes, which serve as exceptional archives and "natural laboratories" for studying sediment–water interactions under a semi-arid climate [1–5]. The region's inherent sensitivity to climate change is not only a feature of the past; it is a critical contemporary issue, evidenced by increasing desertification in the area [6–9].

The substratum of the saline lakes in the Danube–Tisza Interfluve is formed by either Pleistocene loess, aeolian sand of Danubian origin, or a mixture of both [1,2,10,11]. The lakes are fed mainly by precipitation and, to a lesser extent, by groundwater seeping into the depressions, which process transports significant quantities of salts with diverse chemical compositions into the lakes [12–16]. Freshwater carbonate formation (e.g., calcareous mud, freshwater limestone, "honeycomb rock") occurs in these lakes, which, based on their organic matter content, can be divided into two types: (1) calcite-dominated carbonates, which have a higher organic content, mostly from peat consisting of reed and sedge remains, with

their precipitation primarily induced by the CO_2 uptake of vegetation; and (2) dolomite-dominated carbonates, which are poor in organic matter, with their formation resulting mainly from inorganic chemical precipitation driven by evaporation [1,2,11,12,17,18].

This study investigates the mineralogical composition of the lacustrine deposits, with a particular focus on the carbonate-rich layers. The first objective is to provide more extensive and precise data on the major and trace elemental distributions, expanding upon previous knowledge in this area [19]. A second objective is to establish a geochemical and mineralogical based zonation, which reflects changes in catchment processes, water chemistry, and redox conditions. A subsequent aim is to compare this zonation with existing records [3,20–23] to produce a comprehensive multi-proxy reconstruction of past environmental dynamics.

2. Materials and Methods

2.1. Study Area and Sampling

Lake Kolon lies in the Danube–Tisza Interfluve, Hungary, near Izsák, within a broad forest–steppe ecotone of the Pannonian biogeographic region. It occupies a former Danubian branch channel now forming a shallow lacustrine–marsh complex, with marsh patches in an abandoned riverbed overlain by sandy skeletal soils (Arenosols), bordered by sand dunes to the west and loess and sandy plateaus to the east [20–25]. Vegetation around Lake Kolon includes extensive reed beds. Gallery forest remnants and notable orchid species occur in the periphery. The site supports rich avifauna and is embedded in a protected landscape (Kiskunság National Park) [23]. Climate in the region is representative of forest–steppe: mean annual temperature ~12.1 °C, annual precipitation ~514 mm (2011–2022), with hot, dry summers, cold winters, and seasonal precipitation maxima in late spring / early summer. The forest–steppe boundary here is thus highly sensitive both to climatic shifts and anthropogenic influence. In the past few years there is a decreasing trend in the water level and precipitation of the area [20–23].

Novel analytical approaches were applied to the same undisturbed cores (N 46°46′12.85″; E 19°20′43.47″), which had previously been utilised for sedimentological, geochemical, pollen, malacological, and macroelement investigations [20–23].

2.2. Applied Methods

A Spectro xSort XRF spectrometer, mounted in a docking station and equipped with a Rhodium (Rh) X-ray tube and a Silicon Drift Detector (SSD), was used to quantify elements ranging from Magnesium (Mg) to Uranium (U). Samples were collected at 2 cm intervals, dried at 105 °C, and subsequently ground to a fine powder [26,27].

Bulk mineralogical composition was determined by X-ray powder diffraction (XRPD) at 2 cm sampling intervals. Samples were first dried at 60 °C for 24 h, then homogenized in an agate mortar and mounted as random powders on a zero-background silicon sample holder [28,29].

The previous age-depth model for the core [22] was constructed for the entire sedimentary sequence, including intercalated sand layers that lacked radiocarbon dates. This approach did not account for variations in sediment accumulation rates associated with different depositional environments. Consequently, it yielded much younger age estimates for the 220–172 cm interval. To establish a more precise chronology for the 280–0 cm interval, the age-depth model was reconstructed using the Bayesian software package rbacon v. 2.5.7 [30,31] in RStudio v. 2025.05.1 [32], with calibration performed against the IntCal20 dataset [33]. All ages presented in this study are reported as median calibrated years before present (cal yr BP).

3. Results

3.1. Mineralogical and Elemental Composition

The sedimentary sequence exhibits a complex mineralogical and geochemical architecture, reflecting changes in lake trophic status, detrital input, and post-depositional processes over the last ~23,600 years. Five Mineralogical and Elemental Zones (MEZs) are defined based on the mineralogical and elemental composition of the samples. These broadly correspond to lithostratigraphic zones defined from lake-phase development but with adjusted boundaries to better characterise geochemical variation (Figures 1 and 2).

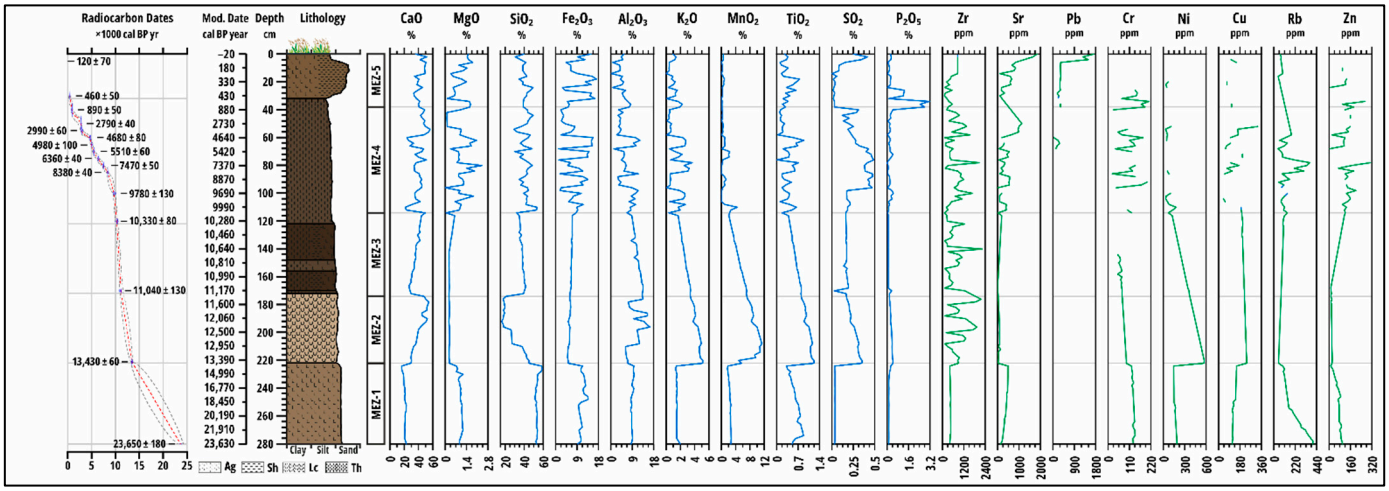


Figure 1. Core profile with newly calibrated ages and major (wt%; blue) and trace (ppm; green) element compositions. Missing values were excluded.

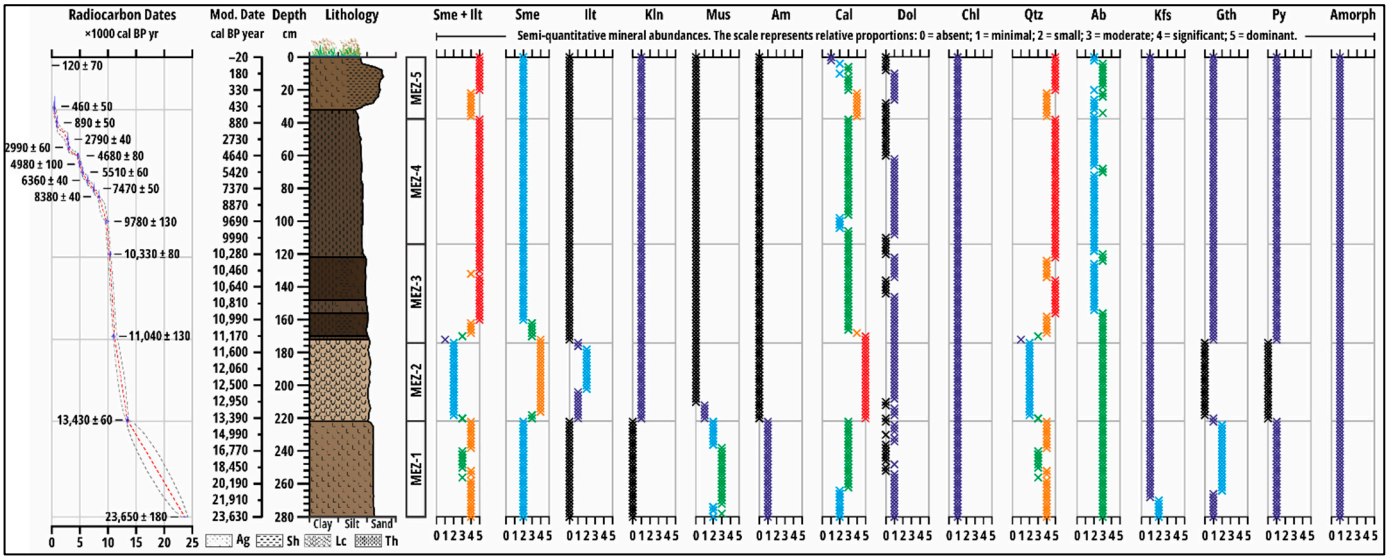


Figure 2. Core profile with newly calibrated ages and semi-quantitative mineral abundances. The scale represents relative proportions: 0 = absent (black); 1 = minimal (purple); 2 = small (cyan); 3 = moderate (green); 4 = significant (orange); 5 = dominant (red).

The mineral assemblage of the sequence is dominated by quartz (Qtz) and calcite (Cal), which together account for the majority of the sediment matrix. Quartz is the principal silicate framework mineral. Its relative abundance fluctuates across the sequence, generally decreasing in carbonate-rich zones and increasing where detrital input dominates or carbonate precipitation declines. Calcite, in contrast, shows pronounced maxima in the mesotrophic lake intervals and a gradual decline towards the fen/peatland zones, reflecting

the influence of carbonate precipitation and hydrological changes. Minor carbonate, in the form of dolomite (Dol), is detected and exhibits erratic variation, indicating either detrital influx or localized diagenetic formation (Figure 2).

Feldspar minerals form a secondary component of the framework silicates. Na-feldspar (albite, Ab) is consistently present throughout the sequence, generally increasing in zones where quartz decreases, suggesting compositional complementarity within the detrital load. K-feldspar (Kfs) is present only in minor amounts and demonstrates limited stratigraphic variability. Amphibole (Am) and muscovite (Mus) are restricted to the lower oligotrophic zone, with muscovite reaching a peak in mid-zone sediments before disappearing upward. These minerals are absent in all subsequent zones (Figure 2).

The phyllosilicate fraction is dominated by smectite (Sme) and smectite–illite mixed-layer phases (Sme+Ilt), particularly where authigenic formation under lacustrine conditions is likely. Chlorite (Chl) exhibits a gradual increase upwards, suggesting progressive detrital contribution or minor diagenetic transformation. Illite (Ilt) and kaolinite (Kln) appear primarily in the mesotrophic and fen/peatland zones, reflecting shifts in detrital supply or weathering intensity. Minor quantities of muscovite (Mus) persist only in the lower oligotrophic zone, while goethite (Gth) and pyrite (Py) occur intermittently, reflecting redox-sensitive conditions, with goethite generally associated with periods of subaerial exposure or oxidation, and pyrite indicative of anoxic conditions. Amorphous material, likely volcanic glass or secondary alteration products, is detected in trace amounts and shows a subtle increase in zones with high detrital influx.

The median abundances of the major rock-forming oxides, expressed in descending order, are SiO_2 > CaO > Al_2O_3 > Fe_2O_3 > MnO_2 > K_2O > MgO > TiO_2 > P_2O_5 > SO_2 (Figure 1, Table 1). The geochemical composition mirrors the mineralogical patterns, displaying broad stratigraphic trends and finer-scale variability. SiO_2 dominates throughout, reflecting detrital quartz input, with maxima in oligotrophic and fen intervals and minima in carbonate-rich zones. CaO is highly variable, peaking in mesotrophic, carbonate-rich intervals (MEZ-2) and showing an inverse relationship with SiO_2, highlighting anti-phased detrital versus authigenic carbonate input. Al_2O_3 and K_2O are relatively stable, while Fe_2O_3, MnO_2, TiO_2, and MgO exhibit zone-specific fluctuations linked to detrital load, oxidation state, and carbonate variation. P_2O_5 and SO_2 remain low, with local maxima reflecting organic matter input or sulphide formation (Figure 1, Table 1).

Table 1. Minimum, maximum, median and average % values of major elements (280–0 cm).

Weight %	Minimum	Maximum	Median	Average
CaO	16.33	56.25	36.42	35.76
MgO	0.01	2.40	0.67	0.74
SiO_2	16.16	58.91	39.94	40.49
Fe_2O_3	1.18	17.13	6.90	8.20
Al_2O_3	0.18	16.43	8.78	8.35
K_2O	0.02	5.14	1.75	2.13
MnO_2	0.01	11.36	2.41	3.32
TiO_2	0.01	1.22	0.57	0.58
SO_2	0.003	0.49	0.17	0.18
P_2O_5	0.01	3.16	0.15	0.26

Trace elements show distinct stratigraphic trends: Zr peaks indicate detrital zircon input, Rb tracks K-bearing silicates and clays, and Sr reflects carbonate accumulation.

Redox-sensitive elements (Cu, Ni, Cr) vary with detrital influx and redox conditions. Pb is confined to the upper fen/peatland intervals, consistent with surface enrichment, while Zn remains low except for sporadic peaks in the uppermost sediments (Figure 1, Table 2).

Table 2. Minimum, maximum, median and average ppm values of trace elements (280–0 cm).

Concentration (ppm)	Minimum	Maximum	Median	Average
Zirconium (Zr)	112	2230	464	676
Strontium (Sr)	11	1830	200	318
Lead (Pb)	40	1720	317	421
Chromium (Cr)	21	210	100	105
Nickel (Ni)	30	573	183	243
Copper (Cu)	40	330	198	172
Rubidium (Rb)	42	402	92	119
Zinc (Zn)	6	310	75	77

3.2. MEZ-1 (280–224 cm; c. 23,600–13,400 cal BP)

This zone correlates with the oligotrophic lake phase, which is dominated by SiO_2 that constitutes over half of the bulk composition (51–59%) and increases stratigraphically upwards. Al_2O_3 (8.3–9.8%) has a low fluctuation with an overall increasing trend. K_2O (1.3–2%) has low fluctuation as well. P_2O_5 (0.1–0.3%) has an upwards increasing trend. MgO (0.7–1.2%) has a first increasing, then a decreasing trend upwards. Concentrations of CaO (16–23%), MnO_2 (1.7–2.8%), SO_2 (0.03–0.04%) and TiO_2 (0.3–0.9%) display an upward decrease, with minor fluctuations. Fe_2O_3 (9.3–13%) has relatively low fluctuation before peaking at 246–248 cm, after which its concentration declines. MgO concentrations (0.7–1.2%) first increase and subsequently decrease towards the top of the zone.

Zr is stable at the base (422–442 ppm) before peaking at 272 cm and 248 cm (464 ppm) and then decreasing towards the top of the zone (415 ppm). Rb shows a continuous decline from a maximum of 400 ppm to 90 ppm. Similarly, Cr (138 to 120 ppm), Ni (190 to 144 ppm), and Zn (112 to 12 ppm) all decrease upwards. In contrast, Sr concentrations increase steadily through the zone from 140 to 490 ppm, while Cu also shows a slow increasing trend (115 to 151 ppm).

The mineral assemblage is dominated by primary silicates. Quartz decreases from its maximum at the base before stabilising, while Na-feldspar increases and then stabilises. Muscovite and amphibole are present only in this zone, with muscovite peaking mid-zone before both minerals decrease to zero by the upper boundary. Calcite increases to a stable plateau, while dolomite decreases chaotically. Smectite abundance increases then stabilises, while chlorite increases steadily. Illite and kaolinite are absent. Goethite shows cyclic peaks, while pyrite and amorphous material increase slightly.

3.3. MEZ-2 (222–174 cm; c. 13,400–11,400 cal BP)

This zone corresponds to the mesotrophic, carbonate-rich lake phase, which is characterised by abrupt geochemical shifts that define three distinct sub-units: (I) 222–210 cm, (II) 208–196 cm, and (III) 194–174 cm. This zonation is most pronounced in the anti-phased behaviour of SiO_2 and CaO. SiO_2 concentrations decrease stepwise from c. 45% to c. 16% through the sub-units, before fluctuating around 18–20%. In contrast, CaO increases steadily from 29% to a maximum of 54% at 178 cm. A sharp, synchronous reversal occurs from 176 cm, where SiO_2 peaks starts to increase and CaO starts to decrease. Several other elements, including K_2O (peaking at 5.14%), TiO_2 (peaking at 1.22%), SO_2, and P_2O_5, attain

their maximum concentrations at the base of the zone (222–220 cm) before decreasing upwards. MnO_2 peaks later at 208 cm, reaching its highest concentration for the entire sequence (11.36%), then starts to decrease upwards. Fe_2O_3 (5.02–6.33%), Al_2O_3 (6.14–16%), and MgO (0.24–0.29%) concentrations also follow the three-stage pattern observed in the major components.

Zr concentrations increase markedly and become highly variable, peaking at 222 cm (905 ppm), 206–202 cm (1130–1220 ppm), 198-190 cm (1301–1932 ppm), 178 cm (1862 ppm) and reaching a zone maximum of 2163 ppm at 174 cm. Rb drops sharply to c. 50 ppm at 222 cm before beginning a slow, steady increase to 73 ppm. Sr also plummets at the start of the zone (to 21 ppm), showing minor fluctuations and a peak at 212 cm (134 ppm), then a decreasing trend to 27 ppm. Cr concentrations drop at the boundary and continue to decrease (120 to 93 ppm). Conversely, Ni increases abruptly at 222 cm from to a peak of 568 ppm, before beginning a gradual decline. Cu also peaks at the base (235 ppm) and then decreases. Zn remains low throughout the zone (13–23 ppm).

The mineralogy undergoes a fundamental transformation. Calcite abundance increases sharply to a maximum of over 40%, defining the zone. This is accompanied by the complete disappearance of muscovite, amphibole, goethite, and pyrite. Conversely, illite and kaolinite appear for the first time. Smectite abundance increases significantly, while quartz and the combined smectite + illite fraction decrease markedly due to dilution. Chlorite remains stable, while Na-feldspar fluctuates at high levels.

3.4. MEZ-3 (172–116 cm; c. 11,200–10,200 cal BP)

This zone marks the transition from the mesotrophic to eutrophic lake phase and to the onset of fen/peatland conditions, which is generally characterised by a decline in detrital-associated elements. Concentrations of SiO_2 (41% to 34%), Al_2O_3 (13% to 8.45%), K_2O (3.42% to 1.68%), MnO_2 (7.1% to 2.11%), TiO_2 (0.8% to 0.39%), SO_2 (0.19% to 0.16%), and P_2O_5 (declining to 0.09%) all decrease stratigraphically upwards. Conversely, CaO (29% to 42%), MgO (0.26% to 0.62%), and Fe_2O_3 (6.05% to 7.02%) concentrations increase through the zone.

Zr concentrations remain high and variable, with major peaks at 172–170 cm (1260–1561 ppm) 152–144 cm (860–1114 ppm), 140 cm (2230 ppm), 122 cm (1250 ppm). Sr reverses its previous trend, increasing from a sequence minimum of 11 ppm (164 cm) to 192 ppm. Rb also continues its steady increase (to 110 ppm). Cr continues to decrease to 50 ppm (144 cm) and disappears from the record. Ni continues its slow decline to 124 ppm, while Cu also decreases (217 to 196 ppm). Zn begins to increase from its previously low values, reaching 114 ppm by the top of the zone.

Quartz and the smectite + illite fraction increase substantially as the carbonate influence wanes. Calcite abundance decreases significantly. Smectite content declines from its peak in the previous zone. Goethite and pyrite reappear, and kaolinite stabilises at a low, consistent level.

3.5. MEZ-4 (114–40 cm, c. 10,200–800 cal BP)

This zone represents the lower section of the fen/peatland phase and is characterised by significant, high-frequency geochemical variability, where SiO_2 (29–53%) and CaO (21–56%) are displaying a wide and often inverse connection. Fe_2O_3 is also a notable component (1.18–17%), exhibiting multiple prominent peaks. Al_2O_3 concentrations (1.25–12%) are generally lower than in the underlying lacustrine zones but display peaks that typically co-vary with those of MnO_2, K_2O, TiO_2, and P_2O_5. Concentrations of K_2O and MnO_2 are substantially reduced overall, although MnO_2 exhibits a distinct peak at 110 cm (reaching 4.47%) and a secondary peak between 74 and 70 cm (up to 2.32%). P_2O_5 concentrations

remain low throughout this sub-zone (0.01–0.46%). SO_2 concentrations exhibit two peaks, one between 96 and 86 cm and a second, higher peak between 76 and 68 cm (reaching a maximum of 0.49%), before declining upwards. MgO concentrations are similarly variable, containing both the sequence minimum (0.01% at 96 cm) and maximum (2.4% at 80 cm).

Zr continues to exhibit multiple, sharp peaks, notably at 104 cm (1103 ppm), 100 cm (1690 ppm), 90 cm (1200 ppm), 78 cm (2060 ppm), 58 cm (1560 ppm), 52 cm (1360 ppm), 44 cm (960 ppm). Sr concentrations are highly variable, with a prominent double peak between 56 cm (980 ppm) and 50 cm (1133 ppm), after which it starts to decrease to 619 ppm. Rb fluctuates and shows multiple peaks, greatest between 84 and 76 cm at 370 ppm, before declining. This is the first zone where Pb is detected, appearing between 68 and 60 cm (40–280 ppm) before disappearing again. Cr (21–200 ppm), Ni (20–180 ppm), and Cu (40–330 ppm) are present only intermittently (hiatuses), with fluctuating values. Zn concentrations are also highly varied (6–310 ppm).

Quartz and the smectite + illite fraction remain the dominant components, exhibiting high but relatively stable abundances. Calcite concentrations are low and variable. Smectite content is low and stable. Goethite and pyrite show a slow, steady increase through the zone.

3.6. MEZ-5 (38–0 cm, from c. 800 cal BP to the Present Day)

This zone represents the uppermost section of the fen/peatland phase, where the geochemistry is inferred to reflect recent environmental conditions and ongoing processes at the sediment–water interface. CaO (33–51%) and SiO_2 (30–49%) remain the dominant components, with significant contributions from Fe_2O_3 (2.85–17%) and Al_2O_3 (0.18–8.44%). Geochemical variability remains high, with most elements exhibiting multiple peaks. MnO_2 concentrations are low (0.01–0.86%) but generally co-vary with K_2O, Al_2O_3, Fe_2O_3, TiO_2, and MgO. P_2O_5 concentrations are generally low (0.03–0.30%) but are punctuated by two peaks at 38–34 cm (3.16%) and 30–26 cm (1.29%). A pronounced geochemical shift occurs at 14 cm. At this horizon, following a period of low concentration from 38 cm downwards, SO_2 values drop to near zero. This corresponds to a sharp decrease in Al_2O_3, K_2O, MnO_2, P_2O_5, and MgO, and a concurrent increase in CaO. This trend reverses in the uppermost 4 cm, where concentrations of SO_2 (0.41%) increase toward the surface, in concert with MnO_2, K_2O, Al_2O_3, Fe_2O_3, TiO_2, and MgO.

Zr values are high but less variable than below, with two smaller peaks at 36 cm (560 ppm) and 26 cm (540 ppm) before stabilising at exactly 860 ppm in the top 14 cm. Sr exhibits peaks (516–660 ppm) before rising to a sequence maximum of 1830 ppm at the top of the sequence. Rb continues its overall decreasing trend, interrupted by a small peak at 14 cm (91 ppm). This zone contains the most significant Pb concentrations, with a median of 320 ppm that perfectly describes the almost stable 38–6 cm interval, and an exceptionally elevated range of 1260–1720 ppm in the uppermost 4 cm. Cr (70–210 ppm) is only present in the lower part of the zone with high peaks, meanwhile Ni (35–70 ppm) is only present at 24–20 cm. Cu (70–210 ppm) and Zn (7–270 ppm) remain highly variable.

Quartz and the combined smectite+illite fraction increase towards the surface. Calcite exhibits a final peak before decreasing sharply in the uppermost sediments. Chlorite and goethite increase towards the surface after a dip. Pyrite steadily increases to the surface.

4. Discussion

4.1. Late Glacial Oligotrophic Lake (c. 23,600–13,400 cal BP Years)

The geochemistry and mineralogy of this zone show a cold, arid, detrital dominated Late Glacial environment. The sediment composition is governed by the influx of physically weathered silicate minerals from the catchment, evidenced by the dominance of silica and

the high concentrations of quartz, feldspars, and associated elements like Al_2O_3, K_2O, Rb, Cr, Ni. The mineralogical assemblage provides clear proxies for the prevailing climate. The initial presence of muscovite and amphibole, minerals relatively susceptible to chemical alteration, confirms a landscape where physical weathering predominated. Their gradual disappearance through the zone, however, signals a subtle but significant climatic shift towards conditions that began to enhance chemical weathering, likely a precursor to the major warming that followed this period. The clay mineralogy reinforces this interpretation; the absence of kaolinite is definitive evidence against warm, humid weathering regimes, while the presence of smectite and illite reflects the specific parent rock composition of the catchment.

In-lake conditions were predominantly oligotrophic and well-oxygenated. However, the iron mineralogy reveals a more complex redox story than simple, persistent oxygenation. The co-existence of both goethite (an iron oxyhydroxide indicating oxic conditions) and pyrite (an iron sulphide indicating anoxic conditions) points to a system with distinct redox micro-environments. The water column itself was likely oxic, allowing for the formation of goethite. The pronounced, cyclic peaks in goethite abundance suggest dynamic, pulsed inputs of dissolved iron from the catchment or periodic enhancements of bottom-water oxygenation. Simultaneously, the minor but persistent presence of pyrite indicates that sulphate reduction was occurring within anoxic niches, likely just below the sediment–water interface where microbial activity, fuelled by a limited supply of organic matter, could deplete oxygen locally.

The carbonate mineralogy also tracks environmental change. Initially low but stable calcite levels are consistent with an oligotrophic lake, with most carbonate being detrital (like the co-occurring dolomite). The subsequent increase in calcite, coupled with the disappearance of dolomite, suggests a shift in the catchment's erosional sources and possibly the first hints of increasing in-lake productivity, a trend that would accelerate dramatically in the next zone.

4.2. Late Glacial Interstadial Productivity Maximum (c. 13,400–11,200 cal BP Years)

This period marks the warming of the Bølling-Allerød interstadial. The geochemical and mineralogical signatures shift fundamentally, driven by rapid climatic amelioration. The primary response was a massive increase in lake productivity. This 'algal bloom' consumed vast amounts of dissolved CO_2, drastically increasing water pH and triggering the precipitation of enormous quantities of fine-grained calcite [11,12,34,35]. This is recorded by the sharp increase in CaO to a sequence maximum of 54% and calcite becoming the single most dominant mineral.

This immense autogenic carbonate production had a diluting effect on all other sediment components. The decreases in SiO_2, Al_2O_3, Rb, and minerals like quartz and clays are not indicative of reduced input, but rather of being overwhelmed by the sheer volume of precipitated calcite. The geochemical changes at the base of this zone—with sharp peaks in K_2O, MnO_2, TiO_2, SO_2, Ni, and Cu— reflects metal scavenging and precipitation at a migrating chemocline in a newly stratified water column. The Cu, however, may also be post-depositional, having been leached from the overlying strata. The complete disappearance of both goethite and pyrite suggests the sedimentary system was entirely reset, with carbonate chemistry now dictating geochemical processes. The complete disappearance of muscovite and amphibole, coupled with the first appearance of kaolinite and illite, signals a fundamental switch in the catchment's weathering regime from physical to intense chemical weathering under warmer and more humid conditions. This period of general warming and humidity appears to have been punctuated by intense aridity. The dramatic increase and high variability of Zr, which is a proxy for the dense mineral zircon

that requires high energy for transport, is strong evidence for enhanced aeolian activity. During dry seasons or multi-annual droughts, reduced vegetation cover on the exposed Danube River alluvial plains would have allowed strong winds to mobilize and transport sand-sized sediment, including zircon, into the basin. This points to a climate of extremes, not simple uniform warmth.

4.3. Paleoenvironmental Transition and Eutrophication (c. 11,200–10,200 cal BP Years)

This transitional zone captures the critical environmental shift at the dawn of the Holocene, chronicling the final stage of the open-water lake and its rapid terrestrialisation into a fen. The primary driver of this transformation was the establishment of a warmer, more stable climate, which initiated a cascade of interconnected responses in both the surrounding catchment and the water body itself.

The geochemical signature reflects a landscape undergoing rapid stabilisation. The marked decline in detrital-associated elements (SiO_2, Al_2O_3, K_2O, TiO_2) and their corresponding trace elements (Ni, Cu) does not signify a reduction in weathering, but rather a fundamental change in erosional processes. The expansion of forests and dense ground cover across the catchment, fostered by the warmer climate, effectively anchored soils and reduced the physical transport of mineral matter into the basin. The disappearance of Cr from the record further underscores this shift in sediment sourcing.

Simultaneously, the lake itself was becoming shallower and significantly more productive—a process of natural eutrophication. The constant presence of and increase in CaO, MgO, and Sr points towards a carbonate-rich mud typical of shallow, productive, hardwater wetlands. This process is often biologically mediated by macrophytes such as *Chara*, which encrust themselves with calcite in sunlit shallow waters [22,23].

The system was no longer overwhelmed by calcite precipitation, allowing other sedimentary processes to re-assert themselves. The rebound in the abundance of quartz and the combined smectite+illite fraction reflects the relative decrease in carbonate dilution. Crucially, the reappearance of goethite and pyrite signifies the re-establishment of complex redox gradients. As the fen developed and organic matter accumulated, distinct oxic zones (favouring goethite) and anoxic zones (favouring pyrite) formed within the sediment profile, a hallmark of productive wetland ecosystems. The stabilisation of kaolinite at a low but consistent level confirms that the catchment was now under a long-term, warm, and humid Holocene weathering regime. However, the persistent high concentrations and sharp peaks of Zr introduce a vital nuance. These Zr peaks, representing aeolian transport of the heavy mineral zircon, indicate that significant, periodic droughts still affected the wider region.

4.4. Established Holocene Fen Environment (c. 10,200–800 cal BP Years)

This long period represents the mature, established fen ecosystem, and its geochemistry is primarily a record of local hydrological variability rather than major regional climate shifts. The defining characteristic of this zone is the high-frequency, inverse cycling of CaO/calcite and SiO_2/quartz. This pattern is a classic signature of a fluctuating water table in a wetland environment [36,37]. During wetter climatic phases or periods of higher groundwater levels, shallow, open-water pools would have expanded across the fen. These pools, rich in dissolved calcium and bicarbonate, would have supported blooms of calcareous mud-producing algae and charophytes, leading to the deposition of sediments rich in CaO and Sr. Conversely, during drier phases, the water table would have lowered, exposing the peat and calcareous mud surfaces at the margins of the pools to desiccation, oxidation, and erosion. Runoff from these erosional events would have delivered siliciclastic material

(quartz, clays) and soil-derived elements into the remaining water bodies, resulting in layers enriched in SiO_2, Al_2O_3, and Fe_2O_3.

The intermittent presence of trace metals like Cr, Ni, and Cu likely reflects these fluctuating redox conditions, where metals could be mobilized during oxidative periods and re-precipitated under anoxic conditions. The sharp peaks in Fe_2O_3 may represent the formation of "bog iron" [38] during particularly intense or prolonged dry spells.

Despite the dominance of local processes, the fen remained connected to the wider regional climate system. The continued occurrence of multiple, sharp Zr peaks throughout this ~9000-year period demonstrates that episodic aridity and strong winds were a persistent feature of the Holocene climate in this region. These events were significant enough to transport dense mineral dust from the Danube floodplains, layering a regional aeolian signal on top of the local hydrological record. The first, transient appearance of Pb in this zone is intriguing; while it could represent a natural enrichment event associated with a specific soil-forming process, its timing makes it a candidate for a very early, low-level anthropogenic signal, possibly from distant, pre-industrial smelting activities whose atmospheric signature was captured by the fen. The slow, steady increase in pyrite throughout this zone also reflects the long-term process of peat accumulation and the establishment of permanent anoxia deep within the sediment profile.

4.5. Recent Fen Dynamics and Anthropogenic Influence (c. 800 cal BP Years to Present Days)

The geochemistry of the uppermost zone is unequivocally dominated by the signature of human activity, marking the local onset of the Anthropocene. The system's natural cycles are sharply disrupted by external inputs. The anomalous P_2O_5 peaks, are far beyond natural background levels [39] and are clear markers of nutrient loading from modern agricultural fertilisers. The Pb profile provides the most striking evidence of industrial impact. Its near-absence in deeper sediments followed by a sharp increase from the mid-20th century, culminating in extreme concentrations of over 1700 ppm in the top few centimetres, is a classic, unambiguous signature of atmospheric pollution from leaded petrol combustion and industrial emissions.

The coherent enrichment of Sr in the same surficial layer further supports an anthropogenic source, as both elements are common tracers of industrial and combustion-derived particulates. These impacts are superimposed on local land-use changes. The pronounced geochemical discontinuity at 14 cm, followed by the surficial increase in SO_2 (from acid rain), redox-sensitive metals (Fe, Mn), and detrital proxies (Al, K, Ti), likely reflects the combined effects of historical peat mining and modern drainage schemes. These activities would have drastically altered the local hydrology, lowered the water table, and exposed previously anoxic sediments to oxidation, thereby mobilising metals and altering the sediment chemistry, a process clearly captured in the final few centimetres of the core.

5. Conclusions

This study employed XRPD and XRF analysis to address a gap in the understanding of lacustrine deposits within the Danube–Tisza Interfluve, a region of critical importance for paleoenvironmental studies in Central Europe. The resulting geochemical and mineralogical record combined with the previous studies [20–23] reveals four distinct environmental phases:

1. The Late Glacial period was characterised by a cold, arid climate and an oligotrophic lake dominated by the influx of physically weathered siliciclastic material, evidenced by a mineral assemblage including muscovite and amphibole.

2. The transition into the Late Glacial Interstadial was an abrupt climatic event marked by a shift to intense chemical weathering and massive endogenic calcite precipitation, punctuated by climatic instability and intense aeolian activity.
3. The Holocene was characterised by the development of a fen with fluctuating water levels, evidenced by the inverse cycling of carbonate and siliciclastic components.
4. The last ~800 years show an undeniable anthropogenic overprint, recorded by sharp peaks in phosphorus from fertilisers and an extreme enrichment of Pb and sulphur from industrial and traffic pollution.

These findings have direct regional and global implications. Regionally, this work provides a detailed terrestrial record for the climatically sensitive Pannonian Basin, demonstrating that the Late Glacial warming was punctuated by extreme arid events driven by aeolian transport from the Danube catchment. This serves as a paleo-analogue for modern climate change, suggesting that rapid warming can increase the frequency of extreme weather. Globally, this study establishes a well-supported, high-resolution environmental timeline, validated by the strong comparability between its geochemical and mineralogical zonation and existing biological records [20–23]. This timeline details major Holocene events, including the onset of peat accumulation and the subsequent atmospheric deposition of industrial pollutants and agricultural fertilisers.

Supplementary Materials: Data can be downloaded at: https://www.mdpi.com/article/10.3390/w17192830/s1.

Author Contributions: Conceptualization, T.Z.V., E.P.-M., G.B. and P.S.; funding acquisition, P.S.; investigation, T.Z.V.; methodology, T.Z.V., G.B. and P.S.; visualization, T.Z.V.; writing—original draft, T.Z.V.; writing—review and editing, T.Z.V.; supervision, E.P.-M. and P.S. All authors have read and agreed to the published version of the manuscript.

Funding: This research received no external funding.

Data Availability Statement: The original contributions presented in this study are included in the article/Supplementary Material. Further inquiries can be directed to the corresponding author.

Acknowledgments: This research was conducted as part of the activities of the Long Environmental Changes Research Group and the Quaternary Research Group at the University of Szeged. The authors gratefully acknowledge the institutional and collegial support that made this work possible.

Conflicts of Interest: The authors declare no conflicts of interest.

References

1. Molnár, B. Földtani kutatások. [Geological Research]. In *Tudományos Kutatások a Kiskunsági Nemzeti Parkban*; HUNGEXPO: Budapest, Hungary, 1985; pp. 29–55. (In Hungarian)
2. Molnár, B. Az alapkutatás szerepe az aktív természetvédelemben. [The Role of Basic Research in Active Nature Conservation]. In *20 Éves a Kiskunsági Nemzeti Park 1975–1995*; Tóth, K., Ed.; Kiskunági Nemzeti Park Igazgatósága: Kecskemét, Hungary, 1996; pp. 98–108. (In Hungarian)
3. Iványosi-Szabó, A. A KNP természetföldrajzi környezete. [Geomorphological Environment of the KNP]. In *20 Éves a Kiskunsági Nemzeti Park 1975–1995*; Tóth, K., Ed.; Kiskunági Nemzeti Park Igazgatósága: Kecskemét, Hungary, 1996; pp. 17–29.
4. Vajda, Z. A KNP Igazgatóság élőhelyeinek bemutatása területenként. [Presentation of the KNP Directorate's Habitats by Area]. In *20 Éves a Kiskunsági Nemzeti Park 1975–1995*; Tóth, K., Ed.; Kiskunági Nemzeti Park Igazgatósága: Kecskemét, Hungary, 1996; pp. 65–68. (In Hungarian)
5. Vajda, Z. A KNP Igazgatóság természetvédelmi kezelésében álló egyéb védett területek. [Other Protected Areas Under the Conservation Management of the KNP Directorate]. In *20 Éves a Kiskunsági Nemzeti Park 1975–1995*; Tóth, K., Ed.; Kiskunági Nemzeti Park Igazgatósága: Kecskemét, Hungary, 1996; pp. 69–73. (In Hungarian)
6. Biró, M.; Molnár, Z. A Duna-Tisza köze homokbuckásainak tájtípusai, azok kiterjedése, növényzete és tájtörténete a 18. századtól. [Vegetation and land-use history in the sand dunes of the Duna-Tisza köze from the 18th century and the mapping of landscape types of the late 18th century]. *Történeti Földrajzi Füzetek* **1998**, *5*, 1–34.

7. Zsákovics, G.; Kovács, F.; Kiss, A.; Pócsik, E. Risk analysis of the aridification-endangered sand-ridge area in the Danube-Tisza Interfluve. *Acta Climatol. Chronol.* **2007**, *40–41*, 169–178.
8. Zsákovics, G.; Kovács, F.; Kiss, A. A szárazodás veszélyének többszempontú térbeli elemzése a Duna-Tisza közén. *Tájökológiai Lapok* **2009**, *7*, 117–126. (In Hungarian) [CrossRef]
9. Meyer, B.C.; Mezősi, G.; Kovács, F. Landscape degradation at different spatial scales caused by aridification. *Morav. Geogr. Rep.* **2017**, *25*, 271–281. [CrossRef]
10. Szilágyi, V.; Gméling, K.; Józsa, S.; Harsányi, I.; Szentmiklósi, L. Oligomictic alluvial aggregates: Petro-mineralogical and geochemical evaluation of sandy gravel formations on the middle course of the Danube (Hungary). *Bull. Eng. Geol. Environ.* **2021**, *80*, 5957–5977. [CrossRef]
11. Molnár, B. Hypersaline lacustrine dolomite formation in the Danube-Tisza Interfluve. *Földtani Közlöny* **1980**, *110*, 45–64. Available online: http://epa.oszk.hu/01600/01635/00229/pdf/EPA01635_foldtani_kozlony_1980_110_1_045-064.pdf (accessed on 15 May 2023). (In Hungarian with English Abstract).
12. Miháltz, I.; Faragó, M.M. A Duna-Tisza-közi édesvízi mészképződmények. [Freshwater Limestone Formations in the Danube-Tisza Interfluve]. In *Az Alföldi Tudományos Intézet Évkönyve 1*; 1946; pp. 371–384. Available online: https://acta.bibl.u-szeged.hu/50411/1/alfoldi_tud_001_371-384.pdf (accessed on 15 May 2023). (In Hungarian)
13. Simon, S.; Mádlné Szőnyi, J.; Müller, I.; Zsemle, F. Identification of near-surface saline water in the Lake Kelemenszék area, Danube-Tisza Interfluve, Hungary. *Cent. Eur. Geol.* **2008**, *51*, 219–230. [CrossRef]
14. Mádlné Szőnyi, J.; Simon, S.; Tóth, J.; Pogácsás, G. Felszíni és felszín alatti vizek kapcsolata a Duna-Tisza közi Kelemen-szék és Kolon-tó esetében. *Általános Földtani Szle.* **2005**, *30*, 93–110. (In Hungarian)
15. Mádlné Szőnyi, J.; Tóth, J.; Pogácsás, G. Soil and wetland salinization in the framework of the Danube–Tisza Interfluve hydrogeologic type section. *Cent. Eur. Geol.* **2008**, *51*, 203–217. [CrossRef]
16. Mádlné Szőnyi, J.; Tóth, J. A hydrogeological type section for the Duna-Tisza Interfluve, Hungary. *Hydrogeol. J.* **2009**, *17*, 961–980. [CrossRef]
17. Jenei, M. Tavi karbonátképződés a Duna-Tisza közén. [Lacustrine Carbonate Formation in the Danube-Tisza Interfluve]. Doctoral Dissertation, University of Szeged, Szeged, Hungary, 2007. (In Hungarian).
18. Kustár, R.; Balázs, R. *Talpalatnyi Kő—Elveszett Emlékeink Nyomában. A Darázskő*; Kiskunsági Nemzeti Park Alapítvány: Kecskemét, Hungary, 2016.
19. Szederkényi, T.; Pál-Molnár, E.; Bertalan, Á.; Kóbor, B. The trace element distribution of lake mud in several hypersaline lakes of the Danube-Tisza Interfluve, South Hungary. *Acta Mineral.-Petrogr.* **2000**, *41*, 147–150. Available online: http://acta.bibl.u-szeged.hu/24898/1/mineralogica_041_147-150.pdf (accessed on 15 May 2023).
20. Sümegi, P.; Molnár, M.; Jakab, G.; Persaits, G.; Majkut, P.; Páll, D.; Gulyás, S.; Jull, A.J.T.; Törőcsik, T. Radiocarbon-Dated Paleoenvironmental Changes on a Lake and Peat Sediment Sequence from the Central Great Hungarian Plain (Central Europe) During the Last 25,000 Years. *Radiocarbon* **2011**, *53*, 85–97. [CrossRef]
21. Sümegi, P.; Molnár, D.; Náfrádi, K.; Makó, L.; Cseh, P.; Törőcsik, T.; Molnár, M.; Zhou, L. Vegetation and land snail-based reconstruction of the palaeocological changes in the forest steppe eco-region of the Carpathian Basin during last glacial warming. *Glob. Ecol. Conserv.* **2022**, *33*, e01976. [CrossRef]
22. Vári, T.Z.; Gulyás, S.; Sümegi, P. Reconstructing the Paleoenvironmental Evolution of Lake Kolon (Hungary) through Integrated Geochemical and Sedimentological Analyses of Quaternary Sediments. *Quaternary* **2023**, *6*, 39. [CrossRef]
23. Vári, T.Z.; Pál-Molnár, E.; Sümegi, P. Reconstructing the Paleoenvironmental Evolution of Lake Kolon (Hungary) through Palaeoecological, Statistical and Historical Analyses. *Diversity* **2023**, *15*, 1095. [CrossRef]
24. Molnár, B. *The Geology and Hydrogeology of Kiskunsági (Little Cumanian) National Park*; JATE Press: Szeged, Hungary, 2015; p. 534. (In Hungarian)
25. Molnár, B.; Iványosi-Szabó, A.; Fényes, J. Die Entstehung des Kolon-Sees und seine limnogeologische Entwicklung. *Hidrol. Közlöny* **1979**, *59*, 549–560. (In Hungarian with German Summary)
26. Tapody, R.O.; Sümegi, P.; Molnár, D.; Karlik, M.; Törőcsik, T.; Cseh, P.; Makó, L. Sedimentological-Geochemical Data Based Reconstruction of Climate Changes and Human Impacts from the Peat Sequence of Round Lake in the Western Foothill Area of the Eastern Carpathians, Romania. *Quaternary* **2021**, *4*, 18. [CrossRef]
27. Karlik, M.; Gyollai, I.; Vancsik, A.; Fintor, K.; Szalai, Z.; Mîndrescu, M.; Grădinaru, I.; Vágási, S.; Bozsó, G.; Polgári, M.; et al. High Resolution Mineralogical Characterization of Sediments—Lake Bolătău-Feredeu (Romania). *Carpathian J. Earth Environ. Sci.* **2021**, *16*, 199–210. [CrossRef]
28. Körmös, S.; Varga, A.; Raucsik, B.; Lukoczki, G.; Radovics, B.G.; Papp, N.; Futó, I.; Schubert, F. Reservoir heterogeneity of an Eocene mixed siliciclastic-carbonate succession, northern Pannonian Basin. *Mar. Pet. Geol.* **2023**, *147*, 105984. [CrossRef]
29. Poppe, L.J.; Paskevich, V.F.; Hathaway, J.C.; Blackwood, D.S. *A Laboratory Manual for X-Ray Powder Diffraction*; Open-File Report 01-041; U.S. Geological Survey: Reston, VA, USA, 2001; p. 88.

30. Blaauw, M.; Christen, J.A. Flexible paleoclimate age-depth models using an autoregressive gamma process. *Bayesian Anal.* **2011**, *6*, 457–474. [CrossRef]
31. Rbacon: Age-Depth Modelling Using Bayesian Statistics. Available online: https://cran.r-project.org/web/packages/rbacon/index.html (accessed on 8 July 2025).
32. RStudio Desktop—Posit. Available online: https://posit.co/download/rstudio-desktop/ (accessed on 15 May 2023).
33. Reimer, P.; Austin, W.; Bard, E.; Bayliss, A.; Blackwell, P.; Ramsey, C.B.; Butzin, M.; Cheng, H.; Edwards, R.L.; Friedrich, M.; et al. The IntCal20 Northern Hemisphere Radiocarbon Age Calibration Curve (0–55 cal kBP). *Radiocarbon* **2020**, *62*, 725–757. [CrossRef]
34. Molnár, Z.; Pekker, P.; Dódony, I.; Pósfai, M. Clay minerals affect calcium (magnesium) carbonate precipitation and aging. *Earth Planet. Sci. Lett.* **2021**, *567*, 116971. [CrossRef]
35. Fodor, M.A.; Ható, Z.; Kristóf, T.; Pósfai, M. The role of clay surfaces in the heterogeneous nucleation of calcite: Molecular dynamics simulations of cluster formation and attachment. *Chem. Geol.* **2020**, *538*, 119497. [CrossRef]
36. Singh, P.; Jiroušek, M.; Hájková, P.; Horsák, M.; Hájek, M. The future of carbon storage in calcareous fens depends on the balance between groundwater discharge and air temperature. *Catena* **2023**, *231*, 107350. [CrossRef]
37. Grootjans, A.P.; Adema, E.B.; Bleuten, W.; Joosten, H.; Madaras, M.; Janáková, M. Hydrological landscape settings of base-rich fen mires and fen meadows: An overview. *Appl. Veg. Sci.* **2006**, *9*, 175–184. [CrossRef]
38. Brenko, T.; Borojević Šoštarić, S.; Ružičić, S.; Sekelj Ivančan, T. Evidence for the formation of bog iron ore in soils of the Podravina region, NE Croatia: Geochemical and mineralogical study. *Quat. Int.* **2020**, *536*, 13–29. [CrossRef]
39. Jalali, M.; Jalali, M.; Beygi, M.; Salehi, Z.; Antoniadis, V. Available and total phosphorus background levels in soils: A calcareous and semi-arid region. *Environ. Monit. Assess.* **2023**, *195*, 600. [CrossRef]

Disclaimer/Publisher's Note: The statements, opinions and data contained in all publications are solely those of the individual author(s) and contributor(s) and not of MDPI and/or the editor(s). MDPI and/or the editor(s) disclaim responsibility for any injury to people or property resulting from any ideas, methods, instructions or products referred to in the content.